J. Fluid Mech. (1977), *vol.* 82, *part* 3, *pp.* 507–528
Printed in Great Britain

The accelerated fully rough turbulent boundary layer

By HUGH W. COLEMAN,
Sandia Laboratories, Livermore, California 94550
ROBERT J. MOFFAT AND WILLIAM M. KAYS
Department of Mechanical Engineering, Stanford University,
Stanford, California 94305

(Received 21 December 1976)

The behaviour of a fully rough turbulent boundary layer subjected to favourable pressure gradients both with and without blowing was investigated experimentally using a porous test surface composed of densely packed spheres of uniform size. Measurements of profiles of mean velocity and the components of the Reynolds-stress tensor are reported for both unblown and blown layers. Skin-friction coefficients were determined from measurements of the Reynolds shear stress and mean velocity.

An appropriate acceleration parameter K_τ for fully rough layers is defined which is dependent on a characteristic roughness dimension but independent of molecular viscosity. For a constant blowing fraction F greater than or equal to zero, the fully rough turbulent boundary layer reaches an equilibrium state when K_τ is held constant. Profiles of the mean velocity and the components of the Reynolds-stress tensor are then similar in the flow direction and the skin-friction coefficient, momentum thickness, boundary-layer shape factor and the Clauser shape factor and pressure-gradient parameter all become constant.

Acceleration of a fully rough layer decreases the normalized turbulent kinetic energy and makes the turbulence field much less isotropic in the inner region (for F equal to zero) compared with zero-pressure-gradient fully rough layers. The values of the Reynolds-shear-stress correlation coefficients, however, are unaffected by acceleration or blowing and are identical with values previously reported for smooth-wall and zero-pressure-gradient rough-wall flows. Increasing values of the roughness Reynolds number with acceleration indicate that the fully rough layer does not tend towards the transitionally rough or smooth-wall state when accelerated.

1. Introduction

Surface roughness can have profound effects on the structure and behaviour of a turbulent boundary layer. A number of experimental investigations in the past have shown that these effects depend on the size, distribution and shape of the roughness elements. The standard procedure has been to lump these parameters into a single characteristic length scale, the equivalent sand grain roughness k_s, evaluated by comparison with the results of the classic experiments on rough pipe flow of Nikuradse (1933). With k_s determined, skin-friction coefficients and mean velocity profiles have been related to a roughness Reynolds number $Re_k = k_s U_\tau/\nu$, where U_τ is the friction velocity. The advent of more sophisticated turbulence models and prediction schemes,

however, has increased the need for more detailed data on the turbulence field. Several previous studies have investigated the structure of fully rough boundary layers (see, for example, Blake 1970; Grass 1971; Pimenta 1975), but no information is available concerning the effects of acceleration and transpiration on the structure.

The rough surface chosen for study in the Stanford programme is a porous flat plate (figure 1, plate 1) composed of uniform (1·27 mm) diameter spheres packed in the most dense array. The roughness is thus deterministic, with a size and distribution describable by a single length scale (the sphere radius r), and the surface elements retain the three-dimensional character of many naturally occurring rough surfaces.

Zero-pressure-gradient results from this programme have been reported by Healzer (1974) and Pimenta (1975). Healzer presented skin-friction data and surface heat-transfer data both with and without blowing for several velocities which included the transitionally rough and fully rough flow regimes. Pimenta reported comprehensive measurements of the fluid dynamics and heat transfer in both transitionally rough and fully rough zero-pressure-gradient layers both with and without blowing.

The present paper reports the fluid-dynamic results of a study of the effects of acceleration on the fully rough turbulent boundary layer. This subject was investigated because of its importance in the flow in nozzles and over turbine blades and re-entry vehicles and also as a logical step in the overall programme by examining the simultaneous effects on the turbulence field of roughness and acceleration both with and without blowing.

Previously published studies of the combined effects of acceleration and roughness on the turbulent boundary layer have reported only values of the wall heat flux. Reshotko, Boldman & Ehlers (1970) and Banerian & McKillop (1974) investigated nozzle wall flows, while Chen (1972) cited experimental results for flow over hemispheres. No boundary-layer information was obtained in these studies.

In the following discussion, the requirements for establishing equilibrium in a fully rough turbulent boundary layer with a pressure gradient and transpiration are developed. Experimental results for both equilibrium and non-equilibrium accelerated layers are then presented and the effects of acceleration and roughness on turbulent boundary-layer behaviour examined.

2. Equilibrium conditions

Background

When a turbulent boundary layer becomes similar in the flow direction, in some non-dimensional sense, it is usually termed an 'equilibrium' flow. The term is generally applied on the basis of similarity in the normalized mean velocity profiles, even though a truly equilibrium turbulent flow should exhibit similarity in both the mean profiles and the turbulence quantities.

Rotta (1950) examined the conditions which would yield a smooth-wall turbulent boundary layer in which the velocity profile was distorted only affinely in the flow direction. He termed such flows 'similar' and showed that, neglecting the viscous wall region, the equations describing the flow become ordinary differential equations if $\frac{1}{2}C_f$ = constant and $U_\infty = ax^m$, where a and m are constants, $\frac{1}{2}C_f = \tau_w/(\rho_\infty U_\infty^2)$ and τ_w is the wall shear stress. For a layer where the friction coefficient is almost independent

of x, similar solutions exist which depend only on m and $\frac{1}{2}C_f$, and the boundary-layer thickness increases linearly with x.

Clauser (1954) presented experimental verification of the existence of similar turbulent boundary-layer flows on smooth walls for two different adverse pressure gradients. He termed such behaviour 'equilibrium' and defined it as the case where both a shape factor

$$G = \left(\frac{H-1}{H}\right)\frac{1}{(\frac{1}{2}C_f)^{\frac{1}{2}}} \tag{1}$$

and a pressure-gradient parameter $\beta = (\delta'/\tau_w)\,dP/dx$ were independent of x. The boundary-layer shape factor H is defined as the ratio of the displacement thickness δ_1 to the momentum thickness δ_2. In a later paper, Clauser (1956) showed that the correct choice for the length scale δ' was the displacement thickness, so that

$$\beta = \frac{\delta_1}{\tau_w}\frac{dP}{dx}. \tag{2}$$

It should be noted that Clauser's shape factor G is identical with that presented earlier by Rotta (1950, 1955).

In a definitive discussion of equilibrium turbulent boundary-layer flow, Rotta (1962) showed that the conditions required for exact equilibrium behaviour (reduction of the equations of motion to an ordinary differential equation) are

$$\tfrac{1}{2}C_f = \text{constant}, \tag{3}$$

$$d\delta_1/dx = \text{constant}, \tag{4}$$

$$\beta = \text{constant}. \tag{5}$$

Two flows obeying these constraints exactly are flow over a smooth wall with $U_\infty \sim 1/(x_0 - x)$, where $x_0 > x$, and flow over a uniformly rough wall with

$$U_\infty \sim \exp\left(xU_\infty^{-1}\,dU_\infty/dx\right).$$

Other variations of U_∞ were shown either to require the roughness to vary with x or not to satisfy exactly the conditions above.

There are indications based on experimental rough-wall studies that exact equilibrium cases exist for conditions outside the velocity and roughness criteria above. Perry, Schofield & Joubert (1969) found that a zero-pressure-gradient turbulent boundary layer developing over a two-dimensional cavity-type roughness of constant height conformed to Rotta's conditions for self-preserving flow.

The fully rough layer

In order to determine the conditions for which equilibrium will be obtained in a fully rough turbulent boundary layer with a pressure gradient and transpiration, consider the two-dimensional momentum integral equation

$$\tfrac{1}{2}C_f + F = \frac{d\delta_2}{dx} + \delta_2(2+H)\frac{1}{U_\infty}\frac{dU_\infty}{dx}, \tag{6}$$

where the variation of ρ_∞ with x has been neglected, as have the normal Reynolds stresses. The blowing fraction F is defined as $F = \rho_w V_w/\rho_\infty U_\infty$, where V_w is the velocity

of the transpired fluid at the wall. For the zero-pressure-gradient, fully rough state. Healzer (1974) has shown that the skin friction is independent of the Reynolds number and can be functionally represented as

$$\tfrac{1}{2}C_f = f(\delta_2/r, F), \tag{7}$$

where r is a length scale characteristic of the roughness elements and is taken as the sphere radius in this study.

One condition necessary for equilibrium is that $\frac{1}{2}C_f$ be constant. In addition, consider the case of constant F assuming that the functional form of (7) will remain valid for flows with a pressure gradient. Under these conditions, δ_2 is constant and (6) becomes

$$\tfrac{1}{2}C_f + F = (2+H)\frac{\delta_2}{U_\infty}\frac{dU_\infty}{dx} = \text{constant}. \tag{8}$$

Defining a pressure-gradient parameter for fully rough flow as

$$K_r = \frac{r}{U_\infty}\frac{dU_\infty}{dx}, \tag{9}$$

(8) can be written as

$$K_r = \frac{\frac{1}{2}C_f + F}{(2+H)(\delta_2/r)} = \text{constant} \tag{10}$$

for equilibrium conditions. For F and K_r constant, it can also be shown that

$$\beta = -\left(\frac{H}{H+2}\right)\left(\frac{\frac{1}{2}C_f + F}{\frac{1}{2}C_f}\right). \tag{11}$$

For a fully rough flow with constant F and K_r, the layer could be expected to exhibit an equilibrium state for which $\frac{1}{2}C_f$, δ_2, H, G and β are all independent of x. This expectation has been experimentally verified in the present investigation for positive K_r and F. For $K_r < 0$ (adverse pressure gradients) (10) indicates that equilibrium flow is possible only for $F < 0$ (suction). Fully rough flows with K_r and F constant are equilibrium flows in the Rotta sense since (3)–(5) are satisfied.

The variation of the free-stream velocity required for an equilibrium flow is found by integration of (9) with K_r = constant to be

$$U_\infty/U_{\infty,0} = \exp\left[K_r(x-x_0)/r\right], \tag{12}$$

where the subscript 0 indicates the position at which the velocity variation begins. This agrees with Rotta's (1962) result, but from the development above it is clear that fully rough flow is required for the velocity variation (12) to give an equilibrium flow. For transitionally rough flow, $\frac{1}{2}C_f$ is a function not only of δ_2/r and F, but also of U_∞. Thus a constant-K_r flow would not be an equilibrium flow for a transitionally rough turbulent boundary layer.

The equivalent sand grain roughness of the present rough surface according to Schlichting (1968, p. 587) is $1{\cdot}25r$. Hence the conversion of the K_r values reported to values based on k_s is easily made, if needed.

The definition of K_r for fully rough flows is analogous to that of the acceleration parameter used for smooth-wall boundary layers:

$$K = \frac{\nu}{U_\infty^2}\frac{dU_\infty}{dx}. \tag{13}$$

An accelerating turbulent flow on a smooth wall with K = constant (Kays & Moffat 1975) yields a boundary layer with constant Re_{δ_2}. This flow is an equilibrium flow in the sense that mean velocity profiles become similar and G and β are constant, but is not truly an equilibrium flow in the sense of (3)–(5) since $d\delta_1/dx \sim 1/U_\infty^2 \neq$ constant.

3. Experimental apparatus and measurement techniques

The experimental apparatus is a closed-loop wind tunnel using air as both the primary and the transpiration fluid. Air temperature is controlled using water-cooled heat exchangers in both the primary and the transpiration loop. The test section is 2·44 m long, 0·508 m wide and 0·102 m high at its entrance. A flexible Plexiglas upper wall can be adjusted to give the desired variation in U_∞.

The test surface consists of 24 plates each 0·102 m in the axial direction. The plates (figure 1, plate 1) are 12·7 mm thick and uniformly porous. They are constructed of 11 layers of 1·27 mm diameter oxygen-free high conductivity (OFHC) copper spheres packed in the most dense array and brazed together. This configuration produces a rough test surface which is uniform and deterministic. Each plate has individual electrical power and transpiration air controls and thermocouples for determining the plate temperature.

The free-stream velocity at the test-section inlet was nominally 26·8 m/s, with a free-stream turbulence intensity of 0·4 %. All data were taken with a 12·7 mm wide, 0·80 mm high phenolic trip installed 76 mm upstream of the test surface. The turbulent boundary layer was in a fully rough state for all cases reported.

All velocity measurements were made in isothermal flow using linearized constant-temperature hot-wire anemometry. Measurements of U and $\overline{u'^2}$ were obtained with a DISA 55P05 horizontal boundary-layer probe consisting of 5 μm diameter tungsten wire with gold-plated ends. Measurements of $\overline{v'^2}$, $\overline{w'^2}$ and $\overline{u'v'}$ were made with a DISA 55F02 45° slanted probe also consisting of 5 μm diameter tungsten wire with gold-plated ends. The slanted wire could be rotated about the probe axis with stops positioned 45° apart.

The physical size of the test section and the porosity of the plates imposed limitations on the strengths of the accelerations which could be investigated. The height of the tunnel (0·102 m at the nozzle exit) limited both the length and the severity of the acceleration region since interference of the top-wall boundary layer with that on the test surface was carefully avoided. Since the plates were porous, the pressure gradient in the axial direction induced flow through the plates even with the transpiration supply valves closed. No effects of the induced transpiration were apparent in the data. From an analysis of this phenomenon, it was concluded that the quantitative effect of the induced transpiration was negligible, certainly for the mildest acceleration and the blown acceleration runs. The qualitative trends in all the data (and the conclusions drawn from them) are believed to be free of the effects of induced transpiration.

Tabular data listings and details of the experimental apparatus, measurement techniques and qualification tests were given by Coleman (1976).

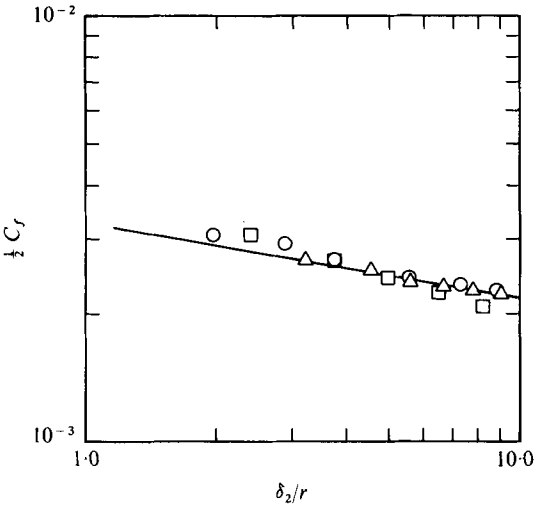

FIGURE 2. Skin-friction coefficients for $K_r = 0$, $F = 0$. ○, present data; △, Pimenta; □, Healzer; ——, equation (14).

4. Results and discussion

The experimental programme covered five different cases:

(1)	$K_r = 0$,	$F = 0$	(baseline),
(2)	$K_r = 0{\cdot}15 \times 10^{-3}$,	$F = 0$	(equilibrium),
(3)	$K_r = 0{\cdot}29 \times 10^{-3}$,	$F = 0$	(equilibrium),
(4)	$K_r = 0{\cdot}29 \times 10^{-3}$,	$F = 0{\cdot}0039$	(equilibrium),
(5)	$K = 0{\cdot}29 \times 10^{-6}$,	$F = 0$	(non-equilibrium).

Case 1 was run as a baseline set and to compare the present data with those of Pimenta (1975) for identical conditions. Cases 2–4 were equilibrium acceleration runs for the fully rough turbulent boundary layer. In case 5 the smooth-wall acceleration parameter $K = \nu U_\infty^{-2} dU_\infty/dx$ was maintained constant. This represents a non-equilibrium run for the fully rough layer.

In setting up each of the equilibrium runs, the value of K_r and the x position at which the acceleration was begun were matched with the δ_2, H and $\frac{1}{2}C_f$ data taken at that position for $K_r = 0$, using (10). Thus the boundary layer entered the region of acceleration near the proper equilibrium state for the K_r applied, and the length of run required to achieve equilibrium was minimized.

Zero-pressure-gradient data

Skin-friction coefficients for case 1 are compared in figure 2 with those reported by Healzer (1974) and Pimenta (1975). Healzer differentiated his momentum-thickness measurements to obtain $\frac{1}{2}C_f$, while the shear-stress method of Andersen, Kays & Moffat (1975) was used in this study and also by Pimenta. The results of Pimenta and the present data show good agreement, while the data of Healzer deviate slightly from the others at the larger values of δ_2/r. The correlation of Pimenta for $1{\cdot}0 < \delta_2/r < 10{\cdot}0$,

$$\tfrac{1}{2}C_f = 0{\cdot}00328(\delta_2/r)^{-0{\cdot}175}, \tag{14}$$

is also plotted.

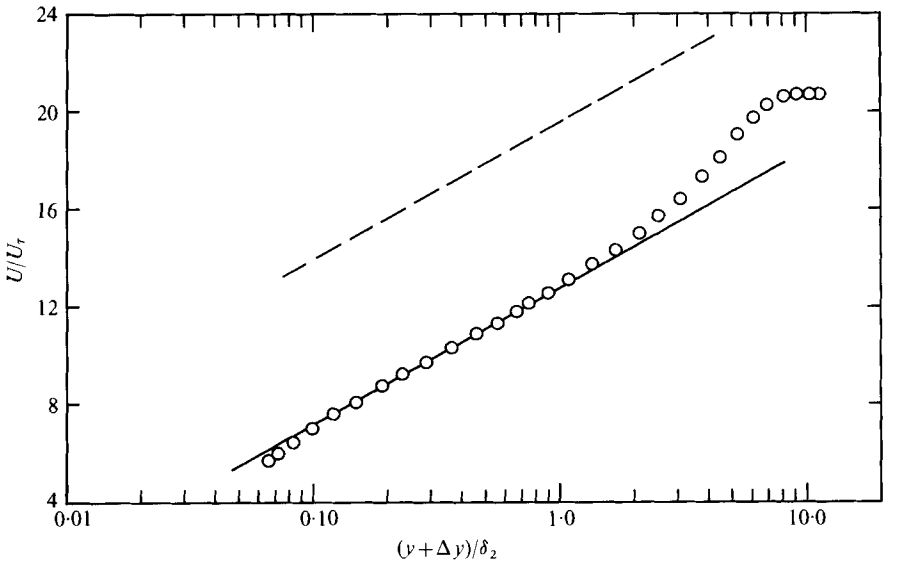

FIGURE 3. Typical mean velocity profile for $K_r = 0$. $\Delta y = 0{\cdot}15$ mm.
——, $U/U_\tau = (0{\cdot}41)^{-1}\ln[(y+\Delta y)/k_s] + 8{\cdot}5$; - - - -, $U/U_\tau = (0{\cdot}41)^{-1}\ln[(y+\Delta y)\,U_\tau/\nu] + 5{\cdot}0$.

The skin-friction coefficients in this study were calculated from

$$\begin{aligned}\tfrac{1}{2}U_\infty^2 C_f = {} & \nu\frac{\partial U}{\partial y}\bigg|_{y_1} - \overline{u'v'}\bigg|_{y_1} - U_\infty U_{y_1} F \\ & - \left[\left(\int_0^{y_1}\left(\frac{U}{U_\infty}\right)^2 dy\right) - \frac{y_1}{2}\right]\left[\frac{U_\infty^2}{\rho_\infty}\frac{d\rho_\infty}{dx} + \frac{2U_\infty^2}{r}K_r\right] \\ & + \left[\int_0^{y_1}\frac{U}{U_\infty}dy\right]\left[\frac{U_\infty U_{y_1}}{\rho_\infty}\frac{d\rho_\infty}{dx} + \frac{U_{y_1}U_\infty}{r}K_r\right] \\ & - U_\infty^2\frac{d}{dx}\left[\int_0^{y_1}\frac{U^2}{U_\infty^2}dy\right] + U_{y_1}U_\infty\frac{d}{dx}\left[\int_0^{y_1}\frac{U}{U_\infty}dy\right]. \end{aligned} \tag{15}$$

To obtain (15), the momentum equation (incorporating the usual boundary-layer assumptions but allowing $\rho_\infty = \rho_\infty(x)$) and the continuity equation are integrated from the surface to a position y_1 in the boundary layer. Then measurement of successive velocity profiles in the x direction and of $\overline{u'v'}$ at $y = y_1$ for each x allows $\frac{1}{2}C_f$ to be calculated. The position y_1 was always 3·30 mm for the data reported, since the rotatable slanted hot wire used to measure $\overline{u'v'}$ was limited to $y > 3{\cdot}18$ mm. Although the axial variation of ρ_∞ was included in the calculations, numerically it was insignificant in all cases in this study.

A typical velocity profile for case 1 is shown in figure 3 *vs.* $(y+\Delta y)/\delta_2$. Since the normal co-ordinate y is referred to the plane of the crests of the spherical elements comprising the test surface, the wall shift Δy gives the location of the 'apparent wall' for the mean velocity. This wall shift was determined by the method suggested by Monin & Yaglom (1971, p. 287). If a logarithmic law-of-the-wall region exists in the velocity profile, it can be shown that

$$\frac{U}{U_\tau} = \frac{1}{\kappa}\ln\left(\frac{y+\Delta y}{z_0}\right), \tag{16}$$

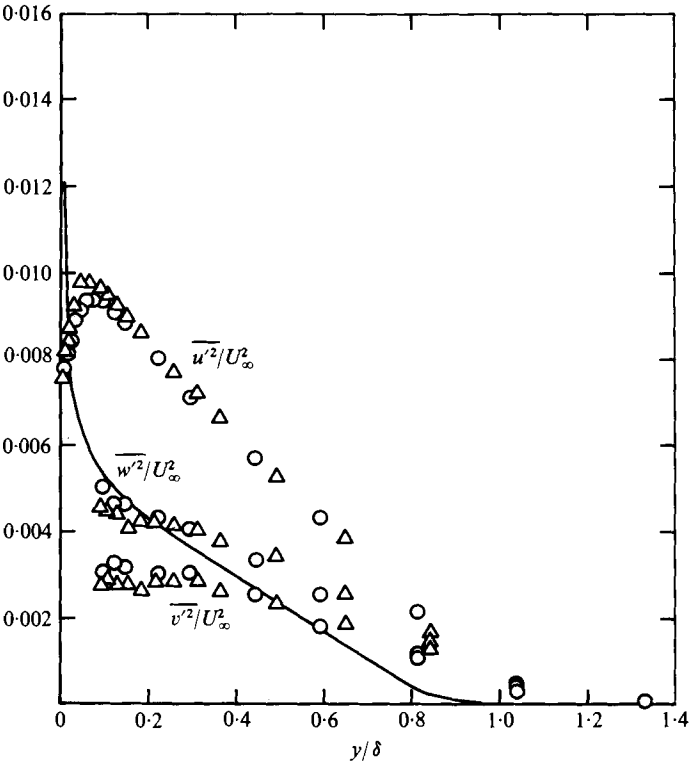

FIGURE 4. Components of turbulent kinetic energy for $K_\tau = 0$. ○, present data; △, Pimenta; ——, $\overline{u'^2}/U_\infty^2$, Klebanoff (smooth wall).

where z_0 and Δy are constants. The value of U_τ being known from the $\frac{1}{2}C_f$ calculations, Δy was varied until a value was determined from (16) for which z_0 was constant.

The present data agree well with Schlichting's (1968, p. 581) expression for fully rough flow

$$\frac{U}{U_\tau} = \frac{1}{\kappa}\ln\frac{y}{k_s} + 8{\cdot}5. \tag{17}$$

The value of k_s used ($1{\cdot}25r$) was determined from Schlichting's value for a geometrically similar surface and not by back-fitting (17). The smooth-wall 'law of the wall' is also shown in the figure for reference.

Measurements of the three components of the turbulent kinetic energy normalized by U_∞^2 are shown in figure 4. The present measurements agree well with those of Pimenta for the same flow conditions. Comparison of the fully rough data with the $\overline{u'^2}$ data of Klebanoff (1955) for a smooth wall shows several important characteristics of fully rough flow (also noted by Pimenta). First, for fully rough flow the peak in $\overline{u'^2}$ is moved out from the wall, lowered and spread over a greater portion of the layer than is the case for smooth-wall flows. Second, the effect of the roughness is felt across practically the entire layer in the form of increased turbulence energy and an altered distribution. This behaviour is also observed in the data of Blake (1970). Thus an assumption that the effect of roughness is confined to the near-wall region is *not* valid for the turbulent kinetic energy components. Pimenta showed that this effect was not

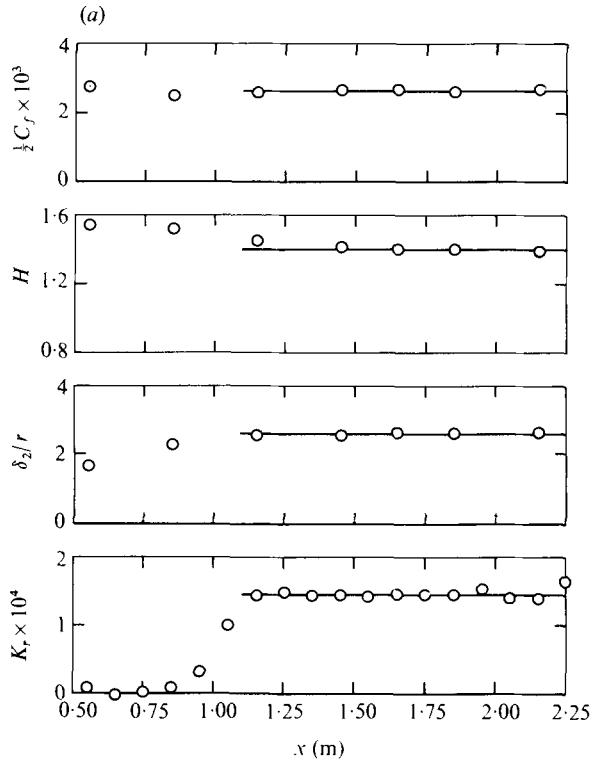

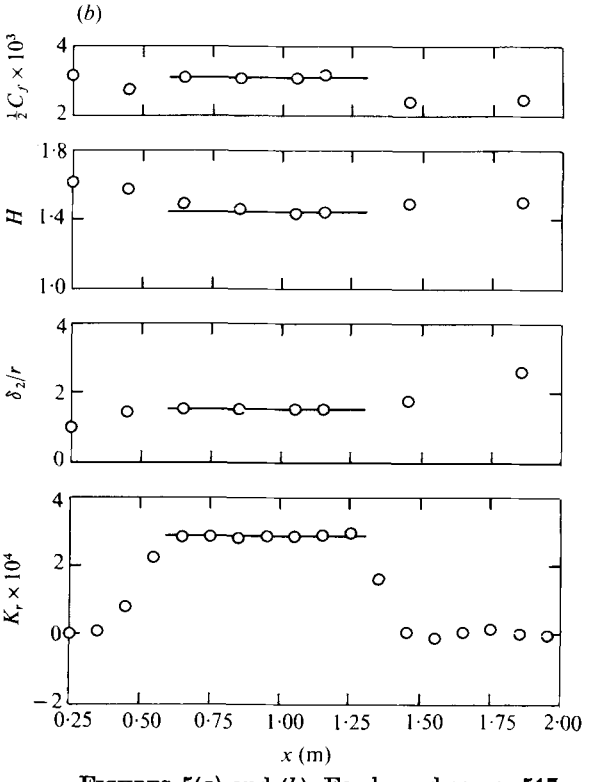

Figures 5(*a*) and (*b*). For legend see p. 517.

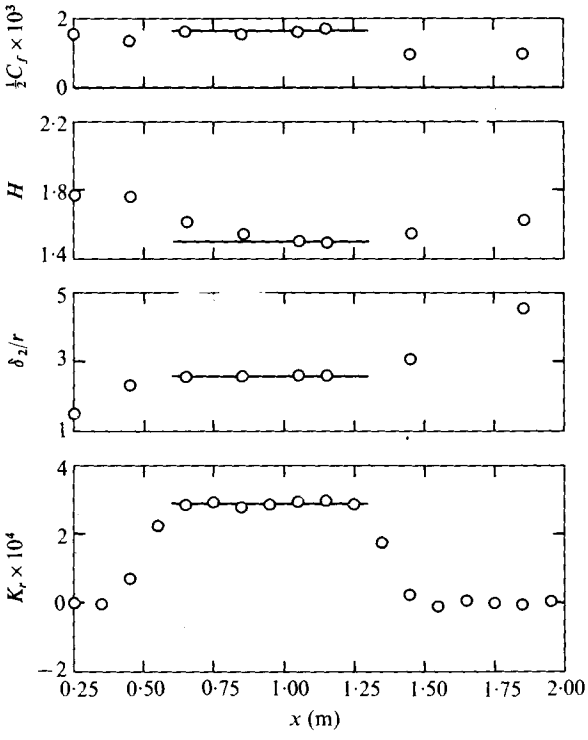

FIGURE 5(*c*). For legend see facing page.

due to the greater free-stream turbulence ($\approx 0{\cdot}4\,\%$) in the present tunnel as compared with that of Klebanoff ($\approx 0{\cdot}02\,\%$). He also showed that the use of U_τ as the normalizing velocity did not collapse the smooth- and rough-wall results, as was suggested by Hinze (1959, p. 490) on the basis of measurements by Corrsin & Kistler (1954) over two-dimensional roughness elements.

Data with acceleration

The behaviour observed for the four cases of accelerated flow investigated is summarized in figures 5(*a*)–(*d*). The variation of K_τ and the response of the integral quantities δ_2, H and $\frac{1}{2}C_f$ are shown *vs.* the distance x along the test section.

In case 2 (figure 5*a*), K_τ was maintained at a constant value of $0{\cdot}15 \times 10^{-3}$ from $x = 1{\cdot}12$ m to $x = 2{\cdot}24$ m, with the free-stream velocity increasing from 26·8 m/s to 35·1 m/s. The momentum thickness, boundary-layer shape factor and skin-friction coefficient all appear to reach constant values in the constant-K_τ region, indicating that equilibrium flow was established. From (1) and (11) it is evident that G and β become constant also. The conditions for exact equilibrium flow given by (3)–(5) are therefore satisfied.

Data for cases 3 and 4, for which a region where $K_\tau = 0{\cdot}29 \times 10^{-3}$ was established, are shown in figures 5(*b*) and (*c*). In case 3, $F = 0$, while in case 4 the blowing fraction had a uniform value ($F = 0{\cdot}0039$) along the entire test section. In both these cases,

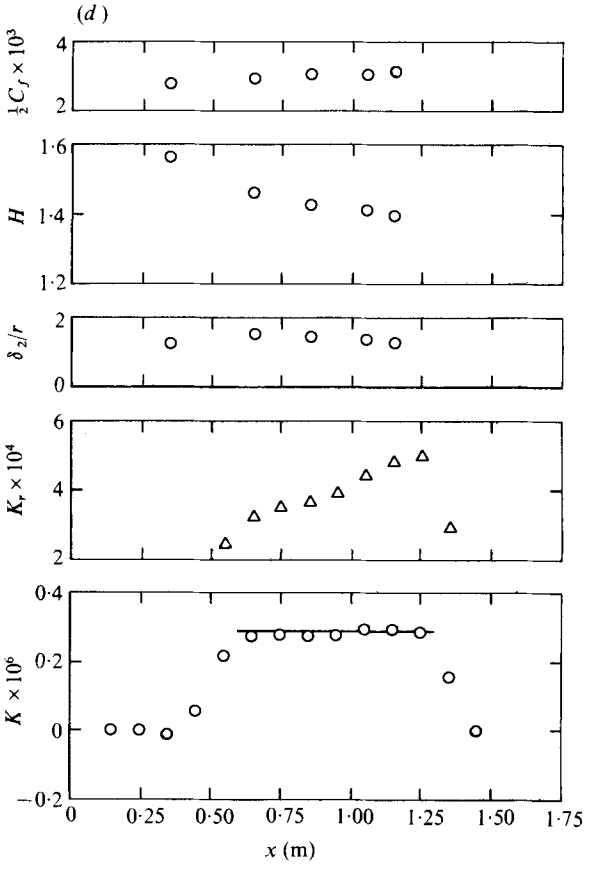

FIGURE 5. Summary data for (*a*) $K_r = 0{\cdot}15 \times 10^{-3}$, $F = 0$, equilibrium acceleration (case 2), (*b*) $K_r = 0{\cdot}29 \times 10^{-3}$, $F = 0$, equilibrium acceleration (case 3), (*c*) $K_r = 0{\cdot}29 \times 10^{-3}$, $F = 0{\cdot}0039$, equilibrium acceleration (case 4) and (*d*) $K = 0{\cdot}28 \times 10^{-6}$, $F = 0$, non-equilibrium acceleration (case 5).

K_r was constant from $x = 0{\cdot}61$ m to $x = 1{\cdot}32$ m. The free-stream velocity increased from 26·8 m/s to 39·3 m/s, and equilibrium flow was observed in the acceleration region, δ_2, H and $\frac{1}{2}C_f$ all approaching constant values.

Data for the $K = 0{\cdot}28 \times 10^{-6}$, non-equilibrium case are presented in figure 5(*d*). The smooth-wall acceleration parameter K was constant from $x = 0{\cdot}61$ m to $x = 1{\cdot}32$ m. The free-stream velocity increased from 26·8 m/s to 45·7 m/s and K_r varied from $0{\cdot}25 \times 10^{-3}$ to $0{\cdot}50 \times 10^{-3}$ in this region. The shape parameter H decreased along the entire test section. The momentum thickness δ_2 increased as the layer entered the region of acceleration, then levelled off and finally decreased. This δ_2 behaviour is similar to that observed by Julien, Kays & Moffat (1969) and Loyd, Moffat & Kays (1970) in an asymptotic accelerated smooth-wall layer. The skin-friction coefficient showed very little variation, and appeared to remain about constant. This is not surprising considering the small variation of the momentum thickness in the acceleration region.

In the acceleration regions of cases 2–4 the equilibrium skin-friction coefficients can be found from (10) rewritten as

$$\tfrac{1}{2}C_f = K_r(2+H)(\delta_2/r) - F. \tag{18}$$

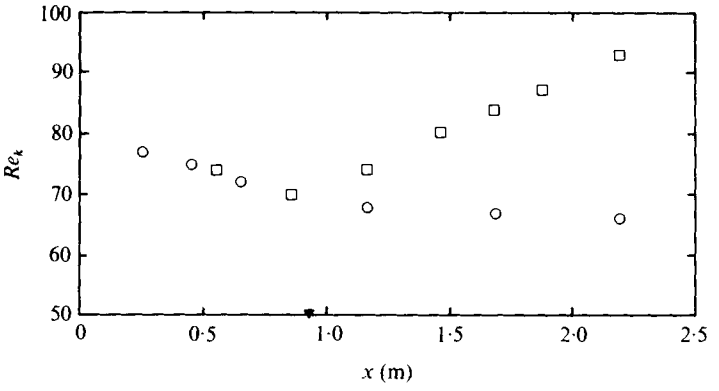

FIGURE 6. Effect of acceleration on roughness Reynolds number. K_r: ○, 0; □, $0{\cdot}15 \times 10^{-3}$. ▼, location where acceleration begins for $K_r = 0{\cdot}15 \times 10^{-3}$.

Values of $\frac{1}{2}C_f$ from (18) agree with those calculated using (15) to within approximately 5% for the unblown cases and 10% for the case $F = 0{\cdot}0039$. When compared in $(\frac{1}{2}C_f, \delta_2/r)$ co-ordinates, the $F = 0$ accelerated data agree to within about 5% with the $K_r = 0$ values.

The variation of the roughness Reynolds number with x is shown in figure 6 for cases 1 and 2. The significant increase in Re_k with acceleration was observed in all accelerated data of this study. This behaviour has important implications. The utility of the roughness Reynolds number lies in its magnitude relative to the thickness of the viscous sublayer. According to the traditional argument, for $Re_k < 5$ the roughness elements do not penetrate the sublayer and the flow retains its smooth-wall characteristics. For $5 < Re_k < 55$–70 (depending on the data and/or author) the flow is 'transitionally' rough, and for $Re_k > 55$–70 the flow is fully rough. These ranges are all for $F = 0$. Since Re_k increases in the acceleration region, the roughness elements protrude further out into the layer (in a non-dimensional sense) in this region. There is no viscous sublayer present in the fully rough layer, so the increase in Re_k with acceleration can be viewed as making it more difficult for a viscous sublayer to form.

This observation is important when one considers the behaviour of accelerated smooth-wall flow. Kays & Moffat (1975) note that experimental evidence indicates that acceleration of a smooth-wall turbulent boundary layer causes an increase in the thickness of the viscous sublayer. In addition, the results of many investigations have shown that acceleration of a smooth-wall turbulent layer causes it to develop towards a state resembling laminar flow. Consideration of these smooth-wall accelerated flow characteristics might lead one to expect a fully rough turbulent boundary layer subjected to a favourable pressure gradient to develop first transitionally rough, then finally smooth-wall characteristics. The present results indicate that this is not the case. On the contrary, acceleration makes a fully rough flow appear 'rougher' in the sense that the roughness elements protrude further, non-dimensionally, into the turbulent layer.

The similarity of mean velocity profiles in an equilibrium acceleration is demonstrated in figure 7 for the case $K_r = 0{\cdot}15 \times 10^{-3}$. Profiles are shown at the three positions $x - x_a = 0{\cdot}56$ m, 0·76 m and 1·07 m, where x_a is the position at which K_r becomes constant. The similarity, extending down to the data point closest to the

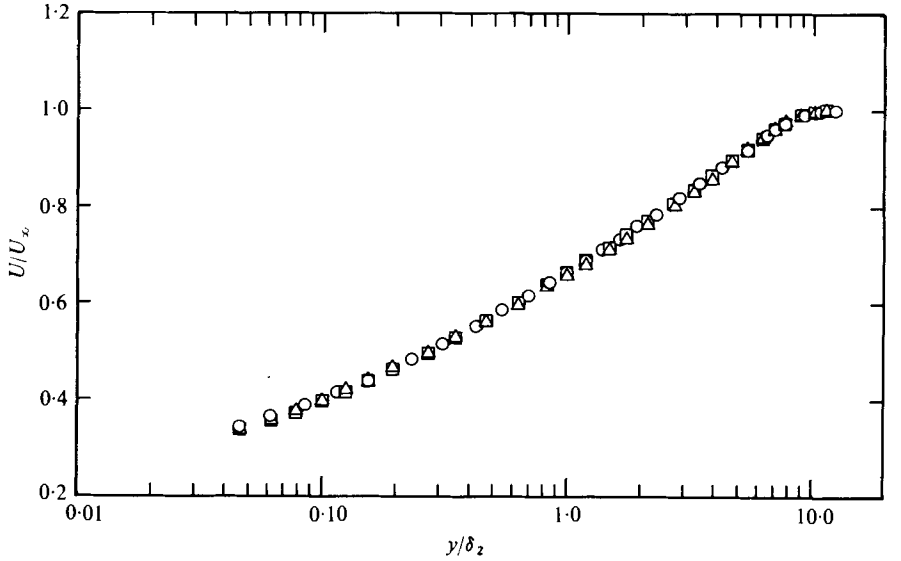

FIGURE 7. Mean velocity profiles illustrating similarity in equilibrium acceleration region ($K_r = 0{\cdot}15 \times 10^{-3}$). $x-x_a$ (m): △, 0·59; □, 0·76; ○, 1·07.

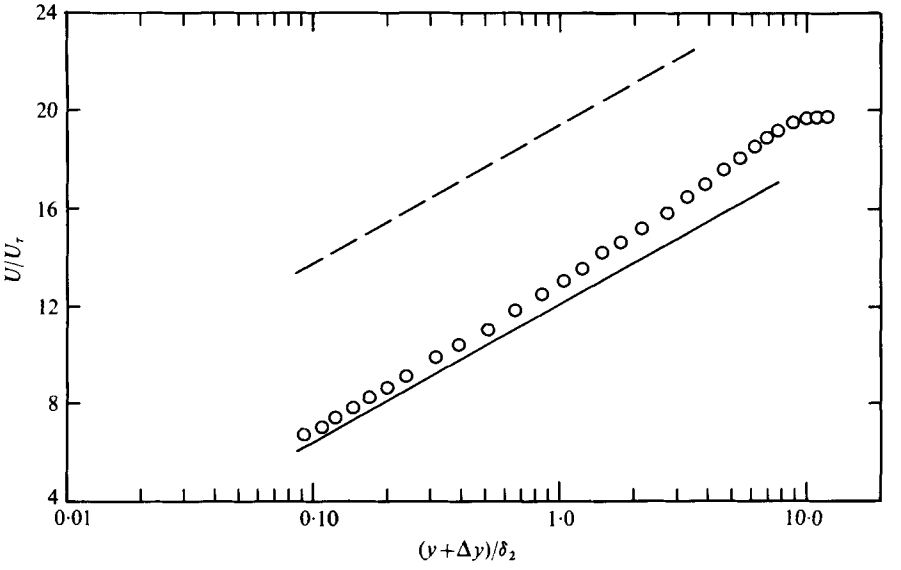

FIGURE 8. Mean velocity profile plotted using shifted wall position. $K_r = 0{\cdot}15 \times 10^{-3}$, $x-x_a = 0{\cdot}76$ m, $\Delta y = 0{\cdot}15$ mm. Curves same as for figure 3.

surface (0·15 mm), was also observed in the other two equilibrium accelerations. As would be expected, no such similarity was observed in the non-equilibrium acceleration.

The mean velocity profile at $x-x_a = 0{\cdot}76$ m from case 2 is plotted in figure 8 in co-ordinates using the wall shift described earlier. The smooth-wall 'law of the wall' and Schlichting's expression (17) for fully rough flow are shown for comparison.

Comparison of the present profile with Schlichting's expression shows that the constant would have to be increased from 8·5 to approximately 9·1 to match the

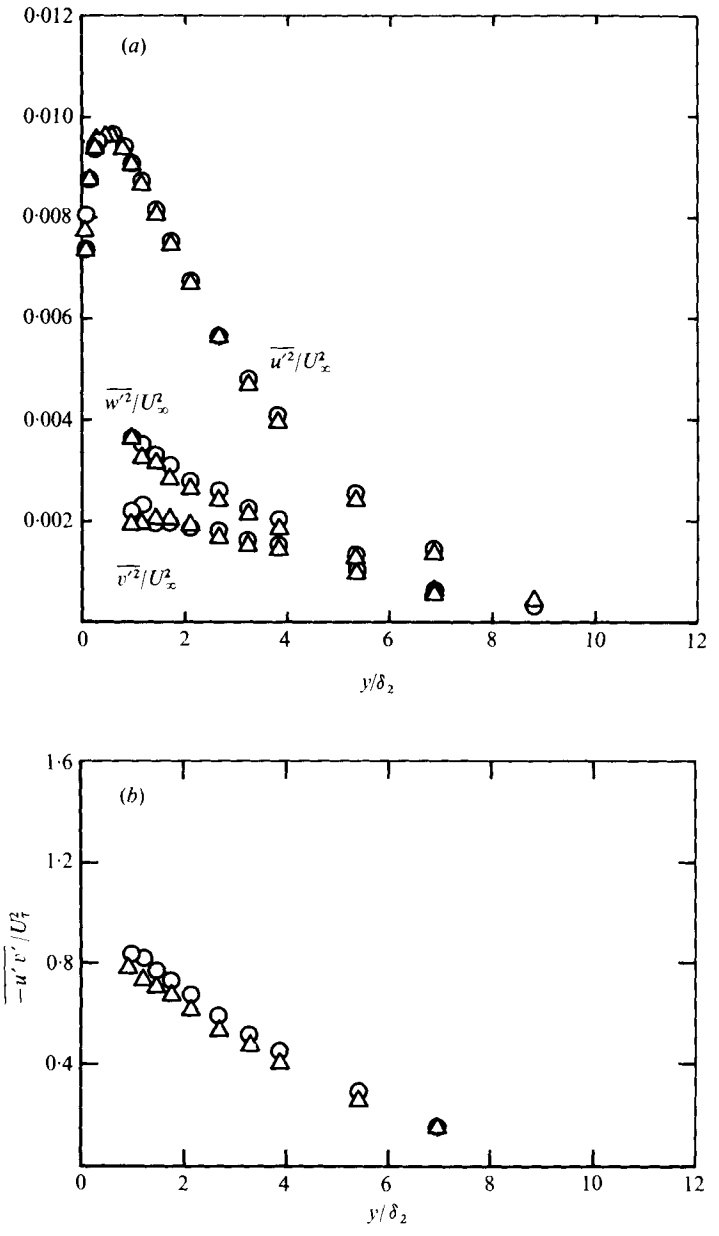

FIGURE 9. Profiles of (*a*) turbulent kinetic energy components, illustrating similarity in equilibrium acceleration region, and (*b*) Reynolds shear stress in equilibrium acceleration region. $K_\tau = 0{\cdot}15 \times 10^{-3}$. $x - x_a$ (m): ○, 0·56; △, 1·07.

accelerated data. The reason for this shift is not known, though it should be remembered that the value 8·5 was determined from Nikuradse's results for flow in a rough pipe. The decrease in the value of $\Delta U/U_\tau$ between the smooth-wall law of the wall and the present data when acceleration is imposed should not, in the authors' opinion, be taken as an indication that the flow is tending towards the transitionally rough state. The $\overline{u'^2}$ profiles presented later exhibit none of the transitionally rough charac-

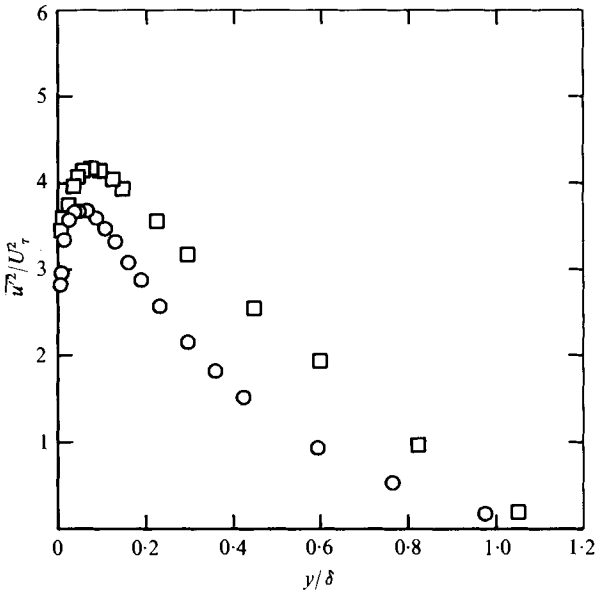

FIGURE 10. Effect of acceleration on $\overline{u'^2}/U_\tau^2$. □, $K_r = 0$; ○, $K_r = 0{\cdot}15 \times 10^{-3}$, $x - x_a = 1{\cdot}07$ m.

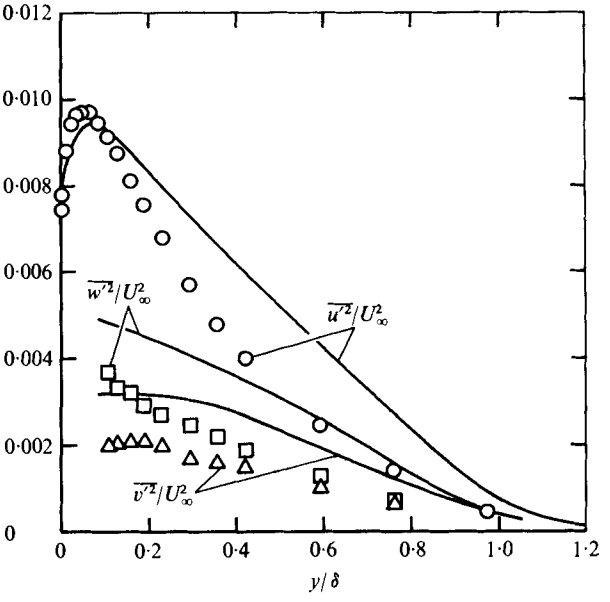

FIGURE 11. Effect of acceleration on the components of the turbulent kinetic energy. ○, □, △, $K_r = 0{\cdot}15 \times 10^{-3}$, $x - x_a = 1{\cdot}07$ m; ——, $K_r = 0$.

teristics described by Pimenta (1975) for zero-pressure-gradient flows on this surface. In addition, the increase in Re_k in the acceleration region indicates a trend away from, rather than towards, the transitionally rough state.

It was found that $\Delta y = 0{\cdot}15$ mm for all the mean velocity profiles in the present unblown cases. Since this is the same as the value found by Pimenta for his zero-

pressure-gradient data, it can be concluded that, for the K_τ range of this study and $F = 0$, Δy is unaffected by favourable pressure gradients and does not vary with x. This result is quite different from that reported by Perry *et al.* (1969), who investigated turbulent boundary-layer flow over two-dimensional roughness elements for both zero and adverse pressure gradients. They found that Δy varied with x, and in fact was actually larger than the roughness height under some adverse-pressure-gradient conditions.

The three components of the turbulent kinetic energy are shown in figure 9(*a*) for the case $K_\tau = 0{\cdot}15 \times 10^{-3}$ at $x - x_a = 0{\cdot}56$ m and 1·07 m. Similarity of these quantities in the flow direction is evident. The Reynolds-stress profiles at the same positions are shown in figure 9(*b*). The difference between the two profiles is of the order of 10%. The results shown in these two figures indicate that the expected state of similarity is being approached by components of the Reynolds-stress tensor, the data suggesting that $\overline{u'v'}$ possibly requires a greater distance than the normal stresses to become truly similar.

The effect of acceleration on the turbulence field is shown in figures 10 and 11. Profiles of $\overline{u'^2}/U_\tau^2$ *vs.* y/δ are shown in figure 10 for the cases $K_\tau = 0$ and $0{\cdot}15 \times 10^{-3}$. The decrease in axial turbulence intensity with acceleration is quite evident and similar to the behaviour observed for accelerated smooth-wall flows by Badri Narayanan & Ramjee (1969). When the profiles are compared in figure 11 (where the data are normalized by U_∞^2), one observes that the peaks in $\overline{u'^2}$ nearly coincide when U_∞^2 scaling is used but are displaced in level if U_τ^2 scaling is used, as was the case in figure 10. This near coincidence of the $\overline{u'^2}$ peaks when normalized by U_∞^2 provides a convenient reference level when comparing the profiles.

All three components of the turbulent kinetic energy for the cases $K_\tau = 0$ and $0{\cdot}15 \times 10^{-3}$ are compared in figure 11 as $\overline{u_i'}/U_\infty^2$ *vs.* y/δ. As stated above, the level of the u' component in these co-ordinates is changed very little by acceleration for $y/\delta < 0{\cdot}1$. The v' and w' components are substantially lower than the $K_\tau = 0$ data in the region $y/\delta \approx 0{\cdot}1$, while in the outer region ($y/\delta \gtrsim 0{\cdot}2$) all three components are lowered by approximately 40% compared with the $K_\tau = 0$ values. Thus, when compared with the unaccelerated data, the level of turbulent kinetic energy is decreased over the entire layer by acceleration and the turbulence structure is much more anisotropic in the inner region. Unfortunately, no measurements of the v' and w' components in a smooth-wall accelerated layer have been reported, so no comparison of rough- and smooth-wall behaviour with acceleration is possible.

The effect of acceleration on the Reynolds shear stress is shown in figure 12, where profiles of $-\overline{u'v'}/U_\tau^2$ are shown for the cases $K_\tau = 0$ and $K_\tau = 0{\cdot}15 \times 10^{-3}$. The behaviour of $\overline{u'v'}$ with acceleration is similar to that calculated by Kearney, Moffat & Kays (1970) for the smooth-wall accelerated layer. No measurements of this term in the smooth-wall accelerated layer have been published to the knowledge of the authors. The observed decrease in $-\overline{u'v'}/U_\tau^2$ with acceleration leads one to expect a probable decrease in the non-dimensional production of turbulent kinetic energy with acceleration.

Consideration of the turbulent kinetic energy equation and the equations for the energies in the three components allows some insight into the behaviour observed in the accelerated turbulent field. The time-averaged turbulent kinetic energy equation

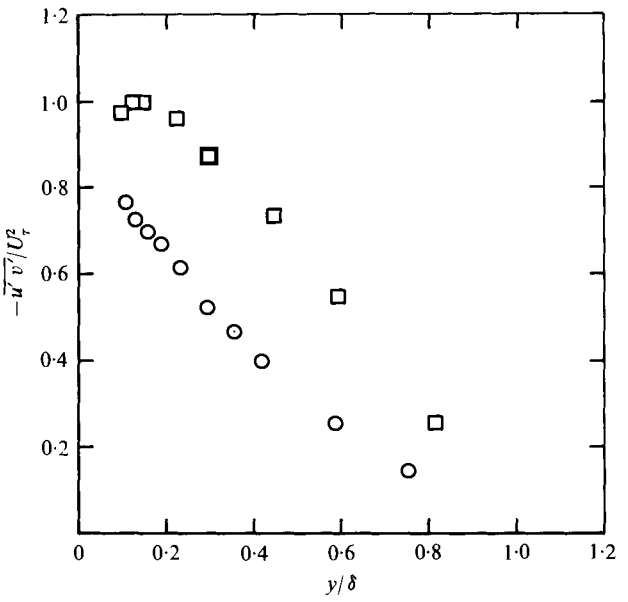

FIGURE 12. Effect of acceleration on the Reynolds shear stress.
□, $K_r = 0$; ○, $K_r = 0{\cdot}15 \times 10^{-3}$, $x - x_a = 1{\cdot}07$ m.

for steady flow without body forces can be written as (see, for example, Monin & Yaglom 1971, p. 381)

$$\frac{\partial}{\partial x_i}(EU_i + \tfrac{1}{2}\rho\overline{u_j' u_j' u_i'} + \overline{p' u_i'} - \overline{u_j' \sigma_{ij}'}) = -\overline{\sigma_{ij}' \frac{\partial u_j'}{\partial x_i}} - \rho\overline{u_i' u_j'}\frac{\partial U_j}{\partial x_i}, \tag{19}$$

where

$$E = \tfrac{1}{2}\rho\overline{u_i' u_i'} = \tfrac{1}{2}\rho q^2$$

and

$$\sigma_{ij}' = \rho\nu(\partial u_i'/\partial x_j + \partial u_j'/\partial x_i).$$

The terms on the left side of (19) are, respectively, the spatial transfer of turbulent kinetic energy per unit volume by the mean motion, by the turbulence fluctuations, by the 'pressure diffusion' and by the viscous shear stresses of the turbulence field. The terms on the right-hand side are the dissipation of E by molecular viscosity and the production of E by the interaction of the Reynolds-stress tensor with the mean velocity gradients.

Figure 13 presents calculations of the turbulent kinetic energy production for Pimenta's zero-pressure-gradient data and the present $K_r = 0{\cdot}15 \times 10^{-3}$ data. From (19), the production term can be written (using the standard boundary-layer assumptions) as

$$\mathscr{P} = -\overline{u'v'}\frac{\partial U}{\partial y} - \overline{u'^2}\frac{\partial U}{\partial x} + \overline{v'^2}\frac{\partial U}{\partial x}. \tag{20}$$

The second and third terms are normally neglected in zero-pressure-gradient flows. In the calculations presented in figure 13, the last term in (20) was neglected since measurements of $\overline{u'^2}$ were made much closer to the wall than those of $\overline{v'^2}$. Thus the results shown present an upper bound on the effect of the pressure gradient through the $\partial U/\partial x$ terms. Values of $\overline{u'v'}$ determined from (15) were used in the calculations

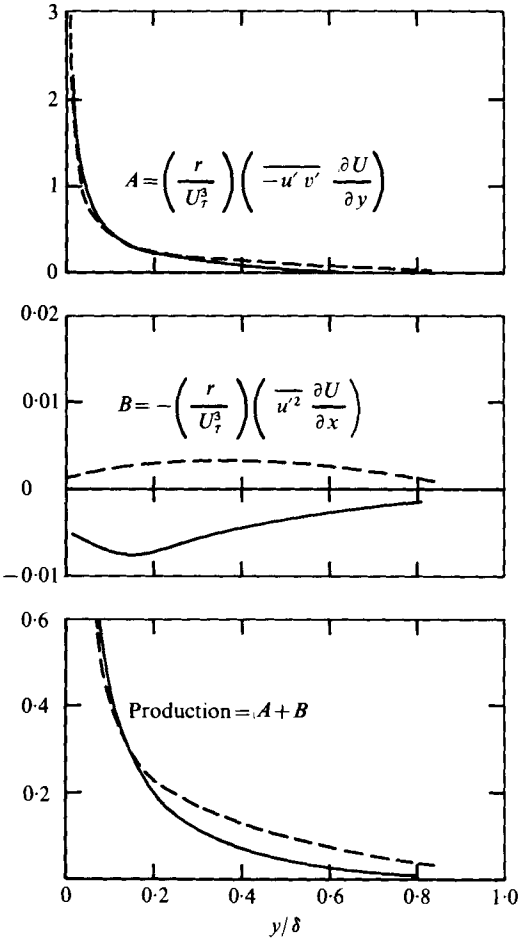

FIGURE 13. Calculated distributions of non-dimensional turbulent kinetic energy production. ——, $K_r = 0{\cdot}15 \times 10^{-3}$; - - - -, $K_r = 0$ (Pimenta).

since comparison with the measured $\overline{u'v'}$ profiles showed agreement to within a few per cent and the calculations from (15) yielded values of $\overline{u'v'}$ closer to the surface than were possible to obtain with the probe.

In a boundary layer subjected to a favourable pressure gradient, the $\overline{u'^2}$ term in (20) is negative and thus appears as a sink of turbulent kinetic energy. Hinze (1959, p. 66) noted that one should expect a decrease in q^2 as a result. Such a decrease in turbulence energy was noted in the present accelerated data (see figure 11, for example). However, the results shown in figure 13 indicate that for the present data the production is decreased with acceleration primarily because of changes in the distributions of $-\overline{u'v'}$ and $\partial U/\partial y$, while the sink term remains of negligible magnitude.

The equations for the three components of E contain terms similar to those in (19) and, in addition, the terms $\overline{p'\,\partial u'/\partial x}$, $\overline{p'\,\partial v'/\partial y}$ and $\overline{p'\,\partial w'/\partial z}$ appear on the right-hand side of the $\overline{u'^2}$, $\overline{v'^2}$ and $\overline{w'^2}$ equations respectively. Since these three additional terms sum to zero by continuity, they do not appear in the equation for the total turbulent kinetic energy. Thus these pressure fluctuation/turbulence field interaction terms

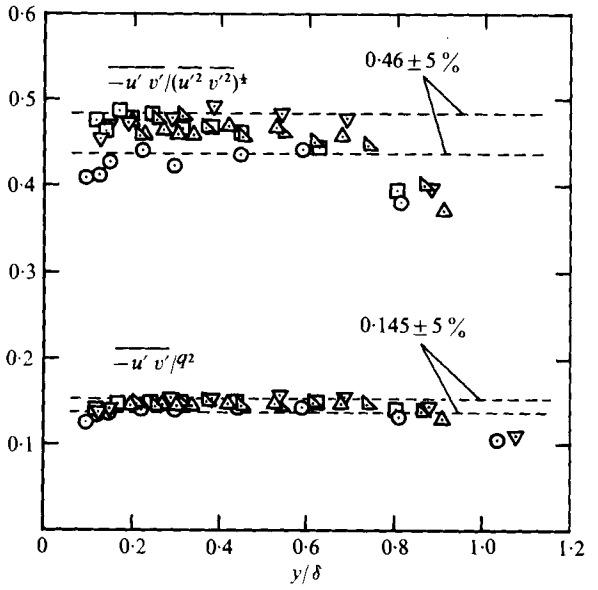

FIGURE 14. Distribution of Reynolds-shear-stress correlation coefficients through the boundary layer. $K_\tau \times 10^3$, F: ○, 0, 0; ⊡, 0·15, 0; △, 0·29, 0; ▽, 0·29, 0·0039. ◺, $K = 0{\cdot}28 \times 10^{-6}$, $F = 0$.

transfer energy among the components of E, but play no direct role in the spatial transfer of turbulence energy.

In the flows of this investigation, all the terms of the production $\overline{u_i'u_j'}\,\partial U_j/\partial x_i$ are negligible except $\overline{u'v'}\,\partial U/\partial y$ (see figure 13). Therefore the entire turbulent kinetic energy production goes into the $\overline{u'^2}$ component of E, and the $\overline{v'^2}$ and $\overline{w'^2}$ components receive energy only through the pressure fluctuation/turbulence field interaction terms described above. Since the effect of acceleration is to make the fully rough layer much more anisotropic in the inner region, acceleration must decrease the sum of the pressure fluctuation transfer (source) and dissipation (sink) terms in the $\overline{v'^2}$ and $\overline{w'^2}$ equations. This argument can be carried further only if one assumes that the dissipation is affected only slightly by acceleration: under this assumption, it would have to be true that the correlations between p' and $\partial v'/\partial y$ or $\partial w'/\partial z$ are decreased significantly by acceleration.

Figure 14 presents the measured correlation coefficients R_{uv} and R_{q^2}, where

$$R_{uv} = -\overline{u'v'}/(\overline{u'^2})^{\frac{1}{2}}(\overline{v'^2})^{\frac{1}{2}} \tag{21}$$

and

$$R_{q^2} = -\overline{u'v'}/q^2. \tag{22}$$

The measured values for all four acceleration cases and the zero-pressure-gradient case are in excellent agreement with those ($R_{uv} \approx 0{\cdot}45$, $R_{q^2} \approx 0{\cdot}15$) reported for both smooth-wall layers (Bradshaw 1967; Orlando, Moffat & Kays 1974) and zero-pressure-gradient rough-wall layers (Pimenta 1975). It thus appears that the relationship between the Reynolds shear stress and the diagonal components of the tensor is truly universal and independent of boundary conditions.

Since the turbulent shear and turbulent kinetic energy are generated primarily during periods of bursting (Kline *et al.* 1967; Kim, Kline & Reynolds 1971), it is

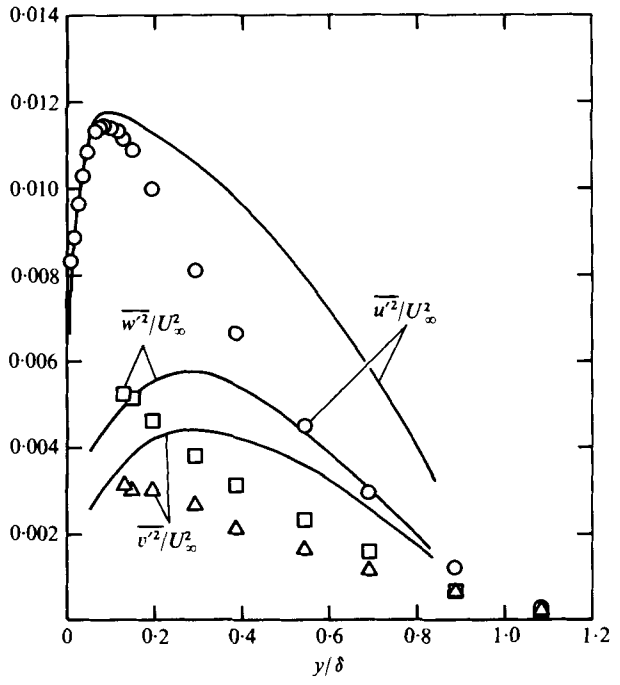

FIGURE 15. Effect of acceleration on the components of the turbulent kinetic energy in blown ($F = 0{\cdot}0039$), fully rough layers. ○, □, △, $K_r = 0{\cdot}29 \times 10^{-3}$, $x - x_a = 0{\cdot}46$ m; ——, $K_r = 0$ (Pimenta).

logical to propose that the apparently universal values of R_{uv} and R_{q^2} observed in boundary layers result from a universal attribute of the bursting and decay process itself. Grass (1971), who reported results of a hydrogen-bubble investigation of a turbulent water channel flow over a pebble-type rough surface, observed that the bursting process appeared to be more vigorous in the fully rough than in the smooth-wall case. The inrushing fluid interacted with the fluid among the roughness elements (which is more energetic than that in the viscous sublayer on a smooth wall), and in the ejection phase of the process the fluid moved almost vertically upwards. These results are consistent with Pimenta's results of higher turbulence energy through the layer in the fully rough state. Thus the *levels* of shear stress and energy are influenced by the vigour of the bursting process and, consequently, the boundary conditions. However, it appears from all the data available that, in any flow where the level of turbulence is generated and maintained by the bursting process, the relationship between the components of the Reynolds-stress tensor is fixed by the basic attributes of the bursting and decay mechanisms and is independent of boundary conditions.

The effects of acceleration on the components of q^2 in a fully rough layer with blowing are shown in figure 15. The data points are for the case $K_r = 0{\cdot}29 \times 10^{-3}$ and $F = 0{\cdot}0039$ of the present study, while the solid lines for $K_r = 0$ and $F = 0{\cdot}0039$ are from Pimenta (1975). Comparison of the two sets of data yields several important points. Acceleration decreases all components of q^2 in the outer region much as it does in the unblown layers. However, the behaviour in the inner region is quite different from that in the unblown cases. The degree of anisotropy in the accelerated data is

about the same at $y/\delta \approx 0{\cdot}2$ as in the zero-pressure-gradient data. Pimenta found that, for $K_\tau = 0$ and fully rough flow, blowing produced a more isotropic turbulence field than that of an unblown layer. It seems probable that blowing and acceleration have opposite effects on the correlations between p' and $\partial v'/\partial y$ or $\partial w'/\partial z$ and thus on the redistribution of energy among the components of q^2. For the present combination of $K_\tau = 0{\cdot}29 \times 10^{-3}$ and $F = 0{\cdot}0039$, it appears that the effects of acceleration and blowing on the turbulence field in the inner region are approximately equal and opposite. Unfortunately, the probe size prevented acquisition of v' and w' data for $y/\delta < 0{\cdot}1$, and the trends inside this region are undetermined.

This work was supported by the Office of Naval Research, Contract N00014-67-A-0112-0072. The experimental apparatus was constructed during an earlier contract from the Department of the Navy, Contract N00123-71-0-0372. The authors wish to thank Dr W. H. Thielbahr, Mr James Patton and Dr Ralph Roberts for their support. The first author also gratefully acknowledges financial support from Sandia Laboratories during the research programme.

REFERENCES

ANDERSEN, P. S., KAYS, W. M. & MOFFAT, R. J. 1975 *J. Fluid Mech.* **69**, 353.

BADRI NARAYANAN, M. A. & RAMJEE, V. 1969 *J. Fluid Mech.* **35**, 225.

BANERIAN, G. & MCKILLOP, A. A. 1974 *Proc. 5th Int. Heat Transfer Conf.* **2**, 234.

BLAKE, W. K. 1970 *J. Fluid Mech.* **44**, 637.

BRADSHAW, P. 1967 *J. Fluid Mech.* **29**, 625.

CHEN, K. K. 1972 *A.I.A.A. J.* **10**, 623.

CLAUSER, F. H. 1954 *J. Aero. Sci.* **21**, 91.

CLAUSER, F. H. 1956 *Adv. in Appl. Mech.* **4**, 1.

COLEMAN, H. W. 1976 Ph.D. thesis, Mech. Engng Dept., Stanford University. (See also *Mech. Engng Dept. Rep.* HMT-24.)

CORRSIN, S. & KISTLER, A. L. 1954 *N.A.C.A. Tech. Note* no. 3133.

GRASS, A. J. 1971 *J. Fluid Mech.* **50**, 233.

HEALZER, J. M. 1974 Ph.D. thesis, Mech. Engng Dept., Stanford University. (See also *Mech. Engng Dept. Rep.* HMT-18.)

HINZE, J. O. 1959 *Turbulence.* McGraw-Hill.

JULIEN, H. L., KAYS, W. M. & MOFFAT, R. J. 1969 *Mech. Engng Dept., Stanford Univ. Rep.* HMT-4.

KAYS, W. M. & MOFFAT, R. J. 1975 In *Studies in Convection*, vol. 1: *Theory, Measurements and Applications*, p. 223. Academic Press. (See also *Mech. Engng Dept., Stanford Univ. Rep.* HMT-20.)

KEARNEY, D. W., MOFFAT, R. J. & KAYS, W. M. 1970 *Mech. Engng Dept., Stanford Univ. Rep.* HMT-12.

KIM, H. T., KLINE, S. J. & REYNOLDS, W. C. 1971 *J. Fluid Mech.* **50**, 133.

KLEBANOFF, P. S. 1955 *N.A.C.A. Rep.* no. 1247.

KLINE, S. J., REYNOLDS, W. C., SCHRAUB, F. A. & RUNSTADLER, P. W. 1967 *J. Fluid Mech.* **30**, 741.

LOYD, R. J., MOFFAT, R. J. & KAYS, W. M. 1970 *Mech. Engng Dept., Stanford Univ. Rep.* HMT-13.

MONIN, A. S. & YAGLOM, A. M. 1971 *Statistical Fluid Mechanics*, vol. 1. MIT Press.

NIKURADSE, J. 1933 *N.A.C.A. Tech. Memo.* no. 1292.

ORLANDO, A. F., MOFFAT, R. J. & KAYS, W. M. 1974 *Mech. Engng Dept., Stanford Univ. Rep.* HMT-17.

PERRY, A. E., SCHOFIELD, W. H. & JOUBERT, P. H. 1969 *J. Fluid Mech.* **37**, 383.

PIMENTA, M. M. 1975 Ph.D. thesis, Mech. Engng Dept., Stanford University. (See also *Mech. Engng Dept. Rep.* HMT-21.)

RESHOTKO, M., BOLDMAN, D. R. & EHLERS, R. C. 1970 *N.A.S.A. Tech. Note* D-5887.

ROTTA, J. C. 1950 *N.A.C.A. Tech. Memo.* no. 1344.

ROTTA, J. C. 1955 *J. Aero. Sci.* **22**, 215.

ROTTA, J. C. 1962 *Prog. in Aero. Sci.* **2**, 1.

SCHLICHTING, H. 1968 *Boundary Layer Theory*. McGraw-Hill.

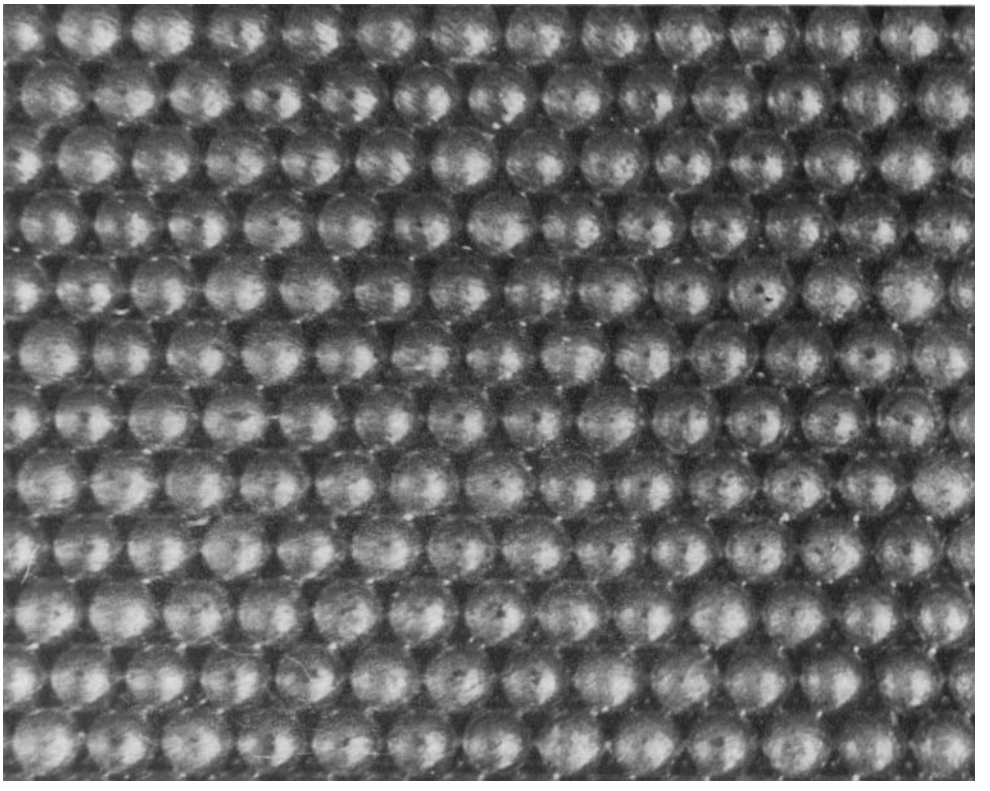

FIGURE 1. Close-up photograph of the rough test surface. Sphere diameter is 1·27 mm.